ACS APPLIED MATERIALS & INTERFACES

Research Article

www.acsami.org

Enhanced Interfacial Adhesion and Osteogenesis for Rapid "Bone-like" Biomineralization by PECVD-Based Silicon Oxynitride Overlays

Azhar Ilyas,[†] Nickolay V. Lavrik,[‡] Harry K. W. Kim,[§,∥] Pranesh B. Aswath,[⊥] and Venu G. Varanasi*[,†]

[†]Department of Biomedical Sciences, Baylor College of Dentistry Texas A&M University, 3302 Gaston Avenue, Dallas, Texas 75246, United States

[‡]Center for Nanophase Materials Science, Oak Ridge National Laboratory, Oak Ridge, Tennessee 37831, United States

[§]Department of Orthopaedic Surgery, University of Texas Southwestern Medical Center at Dallas, Dallas, Texas 75390, United States

[∥]Center for Excellence in Hip Disorders, Texas Scottish Rite Hospital for Children, 2222 Welborn Street, Dallas, Texas 75219, United States

[⊥]Department of Materials Science and Engineering, University of Texas at Arlington, 501 West First Street, Arlington, Texas 76019, United States

ABSTRACT: Structurally unstable fracture sites require metal fixative devices, which have long healing times due to their lack of osteoinductivity. Bioactive glass coatings lack in interfacial bonding, delaminate, and have reduced bioactivity due to the high temperatures used for their fabrication. Here, we test the hypothesis that low-temperature PECVD amorphous silica can enhance adhesion to the underlying metal surface and that N incorporation enhances osteogenesis and rapid biomineralization. A model Ti/TiO_2-SiO_x interface was formed by first depositing Ti onto Si wafers, followed by surface patterning, thermal annealing to form TiO_2, and depositing $SiO_x/Si(ON)_x$ overlays. TEM micrographs showed conformal SiO_x layers on Ti/TiO_2 overlays while XPS data revealed the formation of an elemental Ti−O−Si interface. Nanoscratch testing verified strong SiO_x bonding with the underlying TiO_2 layers. *In vitro* studies showed that the surface properties changed significantly to reveal the formation of hydroxycarbonate apatite within 6 h, and $Si(ON)_x$ surface chemistry induced osteogenic gene expression of human periosteal cells and led to a rapid "bone-like" biomineral formation within 4 weeks. XANES data revealed that the incorporation of N increased the surface HA bioactivity by increasing the carbonate to phosphate ratio. In conclusion, silicon oxynitride overlays on bone-implant systems enhance osteogenesis and biomineralization via surface nitrogen incorporation.

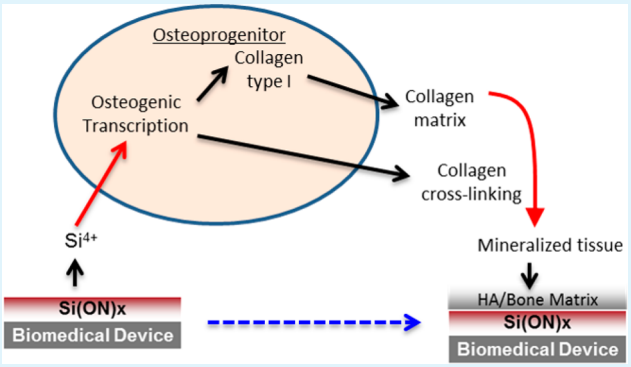

KEYWORDS: *PECVD, qPCR, lithography, periosteal cells, gene expression, hydroxyapatite*

1. INTRODUCTION

Severe bone injuries can occur as a result of traumatic fractures. It is estimated that the incidence of these severe injuries will rise by 400% by 2050 as life expectancy increases.[1,2] These fractures can lead to long hospital stays, delayed bone healing, and permanent injuries that are difficult to heal.[3] These traumatic injuries are challenging to treat due to the large bony defect that needs structural support and osteogenic stimulation during bone healing which can be delayed due to accompanying soft tissue and vascular damage.[4,5] Successful healing of the defect requires that the bony defect be filled with bone graft or bone substitute and fixation device of sufficient strength. Moreover, the healed bone must contain a mineral phase composed of calcium phosphate with incorporated carbonate (hydroxycarbonate apatite or HCA) to maintain biomineral maturity and bioactivity.[6] Another problem plaguing the healing process is time. Smaller defects can be healed with biological bone grafts (autografts and allografts) within 3−6 months.[7] However, biological grafts are limited in supply and cannot structurally support larger fracture sites to facilitate soft callous turnover into bone.[8] Ideally, formation of biomineral (hard callus) within 3−6 months is desired for large defects to reduce the likelihood of inadequate healing.

Current FDA approved biomedical devices for fracture fixation include the use of metal implants, such as titanium (Ti). Ti implants are often used because of their relatively close stiffness match to the surrounding bone.[9] However, these materials do not do anything to promote osteogenesis other than providing fracture stability. Coatings have been attempted to provide an osteoinductive property such that osteogenesis

Received: April 17, 2015
Accepted: June 19, 2015
Published: June 22, 2015

DOI: 10.1021/acsami.5b03319
ACS Appl. Mater. Interfaces 2015, 7, 15368−15379

may be hastened. Yet, these coatings are unsuitable for bone healing. First, synthesis routes for synthetic hydroxyapatite overlay cause inhomogeneity in the coating and have thermal expansion mismatch with the underlying Ti, leading to delamination and instability of the coating.[10] Bioactive glass coatings, which are modified from commercially available bioglass with added MgO for improved thermal expansion matching, have shown a drawback to down-regulate important osteogenic markers associated with bone formation due to Mg^{2+} release.[11] Thus, it is desired that researchers fabricate overlays or coatings that have strong adherence with the underlying metal while providing a stimulatory environment for rapid bone healing.

Preparation of bioactive amorphous silica-based materials by plasma enhanced chemical vapor deposition (PECVD) may improve their performance in applications of bone healing. PECVD is a process technology that uses reagent gas sources to deposit thin films onto substrates of any geometry and size. The film chemistry, thickness, and nanoscale grain size are controlled by reagent chemistry, temperature, and pressure at the reaction surface. PECVD is advantageous because of its low temperature for deposition (<500 °C), which reduces the potential for overlay delamination due to thermal expansion mismatch. The residual stress of the PECVD-based coating varies with the film composition structure, deposition temperature, RF power, pressure, and the nature of the substrate.[12] The coefficients of thermal expansion for Ti-metal and TiO_2 are nearly $8 \times 10^{-6} \times {}^{\circ}C^{-1}$ and $9.5 \times 10^{-6} \times {}^{\circ}C^{-1}$, respectively,[13,14] whereas SiO_2 on Ti-based implants may have thermal expansion coefficients in the range $8-15 \times 10^{-6} \times {}^{\circ}C^{-1}$ depending upon the composition of the SiO_2 layer.[15,16] A low-temperature PECVD process alleviates the issues caused by the lattice constant and thermal expansion coefficient mismatch.[17] Moreover, this low-temperature deposition eliminates the need for added constituents (e.g., MgO) to accommodate thermal expansion mismatch.[18−21]

Attempts to strengthen the amorphous silica network have involved the addition of nitrogen (N) as a constituent to the SiO_x network. The addition of N changes the tetrahedrally coordinated network into one that is a combination of tetrahedral and trigonal.[22] Incorporation of N (through annealing with N_2 gas) into the amorphous silica-based bioactive glass matrix improved its mechanical strength.[23] This also strengthened the amorphous silica-based bioactive glass−Ti interface. However, these coatings are limited in that they can only be applied by enameling, which has a large coating to interface thickness ratio (1000:1) and therefore leaves it more susceptible to delamination.[24] Sputter coated silicon oxynitride films have also been studied for their mechanical properties and showed a linearly increasing strength with N content.[22] Beyond its effect on SiO_x mechanical strength, the effect of adding N on biomineralization and cells' response to $Si(ON)_x$ surfaces are still unknown and will be studied here. Bioinspired surface topographies at nano- and micrometer scales are known to influence cellular behaviors such as cell adhesion, migration, differentiation, and growth.[25−28] The microscale patterns that have gained the maximum interest are regular ridge and groove pattern (micrograting) structures due to its simplicity.[25] Studies show that moderately rough surfaces (1−2 μm) show stronger bone responses than smoother or rougher surfaces.[28] Recently marketed oral implants also have moderately rough surfaces that permit bone ingrowth into minor surface irregularities, promoting osseointegration.[28] while a bioactive coating can add biochemical bonding to biomechanical bonding of these oral implants. Therefore, we will integrate micrograting features with surface chemistry for cell culture studies.

In this study, we hypothesize that amorphous silica-based overlays fabricated through PECVD will have strong adhesion with underlying metal substrates while enhancing osteogenesis to hasten bone matrix formation. We tested the hypothesis by determining (1) the chemical and mechanical properties of the PECVD-based SiO_x-Ti/TiO_2 interface and (2) the effect of $Si(ON)_x$ overlays with textured surfaces on osteogenesis and biomineralization using human osteoprogenitor cells from the periosteum. So, we have two separate aims of this study. Our first aim is to study the potential interfacial adhesion of PECVD amorphous silica-based materials. The second aim is to assess the potential bioactivity of the amorphous-silica-based surfaces as compared to established amorphous-silica-based control surfaces. The outcome from the first aim will give insight into the adhesion strength of PECVD SiO_x-based materials on Ti. The outcome of aim 2 will give insight into the PECVD process and how it can impart bioactive features to SiO_x-based materials as compared to bioinert glass chemistries that may be considered for implant coating applications. The results of this study demonstrate that PECVD amorphous silica-based overlays are strongly adherent to the metal/metal oxide surface, and the surface chemistry enhances the gene expression, collagen formation, and mineral formation by human osteoprogenitor cells *in vitro*.

2. MATERIALS AND METHODS

2.1. Study Design. To test the above hypothesis, this study was carried out in two confluent sections. First, a simulated SiO_x-Ti/TiO_2 interface was fabricated, and its chemical and mechanical properties were investigated to assess interfacial congruity. Si wafers were coated with Ti, followed by optical lithography and plasma etching to define patterns in Ti layer. The wafers were baked to grow a thin TiO_2 layer, and then deposited for the PECVD-based SiO_x overlay. The Ti−TiO_2−SiO_x interface was then extracted using SEM-FIB and imaged using TEM. Milling XPS was used to determine elemental composition through the interface and initial functional group formation after processing. Nanoscale scratch testing was used to determine interfacial adhesion.

In the second part of this study, *in vitro* properties of the amorphous silica-based overlays with varying levels of nitrogen incorporation were tested for their osteogenic effect. Samples of SiO_x, $Si(ON)_x$, and SiN_x coatings were overlaid onto Si substrates by PECVD. No Ti was added so that the effect of varying the chemistry was studied solely when compared to control samples having no Ti involved. Glass coverslips were used as a control material for cell-free and cell culture *in vitro* testing as they do not degrade and have been previously established as an adequate control for cell culture studies.[11,20,29,30] Glass cover slips are also used as a comparative control surface for cell culture to study the osteogenic behavior on various biomaterials including Ti.[31,32] Cell-free immersion testing was conducted to determine *in vitro* degradation behavior using Raman spectroscopy, contact angle measurements, and optical and scanning electron microscopy. Cell culture studies were carried out using the human periosteal cells, which are considered as osteoprogenitor cells since they undergo osteogenic differentiation upon the addition of ascorbic acid and have similar osteogenic markers as osteoblasts[33] and are often assayed for relative gene expression and biomineralization using qPCR, Raman spectroscopy, and optical and scanning electron microscopy.

2.2. Device Fabrication. To create the Ti/TiO_2−SiO_x devices and $Si(ON)_x$ overlays, the processes used were tailored around rapid prototyping of various deposition, etching, and analysis techniques. Figure 1 shows a schematic diagram to demonstrate the step-by-step

DOI: 10.1021/acsami.5b03319
ACS Appl. Mater. Interfaces 2015, 7, 15368−15379

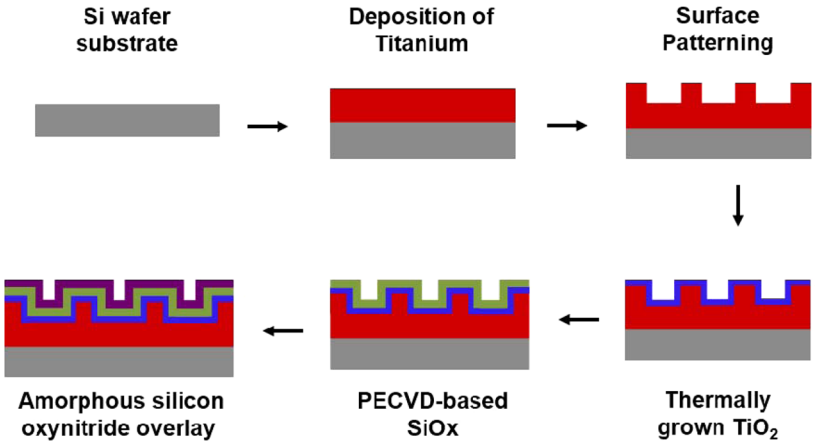

Figure 1. Process flow for the fabrication of $Si(ON)_x$ overlays. A schematic diagram to illustrate the fabrication process for PECVD amorphous silica-based overlays on Ti with Si-wafer substrate.

fabrication process. The fabrication process started with standard cleaning of single crystal Si wafers, which were used as the base substrate. The cleaning process started with immersion of Si wafers in piranha solution ($3H_2SO_4$:$1H_2O_2$) at 95 °C for 10 min followed by rinsing in DI water. This process removed any dust particles and photoresist residues. The wafers were then immersed in NH_4OH, H_2O_2, and DI water mixed in 1:1:10, respectively, for 5−10 min at 70 °C. This process removed any organic film and metal residues. Next, the wafers were cleaned in a solution of HCL, H_2O_2, and DI water mixed in 1:1:10, respectively, for 5−10 min at 80 °C in order to get rid of atomic and ionic contaminants. Finally, the wafers were dipped in buffered hydrofluoric acid (BHF) for about 60 s to remove the native oxide layer. The wafers were then rinsed in DI water followed by nitrogen gas to blow them dry. The wafer were dehydrated for 5 min at 200 °C and allowed to cool down for 1−2 min before proceeding to the next step of Ti deposition. Ti layers are then deposited using electron-beam physical vapor deposition (EB-PVD) system. Photolithography and reactive ion etching (RIE) were deployed for patterning Ti layer to create the desired trench size for cellular studies at a later stage. Thermal oxidation was then employed to create sufficient layer thickness of TiO_2 to anchor overlays. PECVD of amorphous silica-based overlays was then conducted to build SiO_x/$Si(ON)_x$ overlays onto structured Ti/TiO_2 surfaces.

2.2.1. Deposition of Ti Using e-Beam Physical Vapor Deposition (EB-PVD) system. To deposit a uniform layer of Ti on Si wafer, an electron-beam physical vapor deposition system was used. A Ti metal target was used as the Ti source, which was bombarded with the electron beam under high vacuum. The electron beam excited the target and evaporated Ti atoms. These vapors deposited as columnar grains on the Si wafer placed in the vacuum chamber. The emission current was used to control the deposition rate. The deposition was carried out at 1 Å/s at an emission current of 3.1 mA and chamber pressure of 5×10^{-8} Torr to deposit a 300 nm thick layer of Ti.

2.2.2. Surface Patterning. The surface of the Ti layer was patterned to have a textured topography to promote cell migration and extracellular matrix attachment. The surface pattern was carried out through a series of sequential procedures that include mask writing, followed by photolithography and dry etching using RIE process.

a. Mask Writing. Masks for contact photolithography were prepared using a laser mask writer (Heidelberg DWL 66 Direct Write Lithography Tool). A computer-aided design of the desired pattern was developed using AutoCAD software. Using the mask writer, the pattern was then transferred to a photoresist and Cr coated 5×5 in.^{2} glass substrate with 2.4 mm thickness. Mask writing was completed over 36 h.

b. Photolithography. Contact photolithography was used to transfer the mask pattern into a thin photoresist film deposited onto a p-type, (100) orientation, single-side polished silicon wafer of 4-in. diameter and 500 μm thickness. Negative photoresist SU-8 2000 (MicroChem, MA) was applied to the 4-in. wafer with Ti film by using a spin coater. The wafer was properly centered in the middle, and the photoresist was spin coated at 3000 rpm for 30 s to have a uniform layer of resist. Microprime MP-P20 liquid HMDS (Shin-Etsu MicroSi Inc., AZ) was used as an adhesion promoter between the photoresist and the substrate surface. Application of each primer and the resist was done in the center of the spinning wafer in a fluid motion using an eye-dropper without satellite droplets. The wafer with primer and resist coating was baked at 90 °C for 90 s and allowed to cool down for 60 s. The wafer was then exposed to UV light using Quintel Q4000 Mask Aligner (Quintel Contact Lithography Tool). The mask was placed first on the mask vacuum chuck against the banking pins with chrome side facing down. Mask vacuum was turned on to hold the mask, and the wafer was exposed for 8 s in contact mode. A post-exposure bake at 115 °C for 60 s was carried out followed by 1 min cool down cycle. The wafer was subsequently submerged in the SU-8 developer for 60−90 s to get the pattern in photoresist. The wafer was rinsed in DI water and blown dry under a nitrogen gun. The wafer was descumed for 20 s in O_2 plasma using oxford RIE systems (TePla) followed by an aggressive descum cycle at low pressure for 30 s to get a clean patterned wafer.

c. Reactive Ion Etching (RIE). After photolithography, the exposed Ti film was etched using RIE process in order to transfer the photoresist patterns to the underlying Ti film. The Si wafer was placed into the etching chamber, and the system was allowed to pump down to its base pressure ($0.5-1.0 \times 10^{-4}$ Torr). RIE was performed using an Oxford Plasmalab 100 RIE/ICP Etcher for metal etching (Oxford Instruments, U.K.). Within the Oxford RIE system, a Ti etching protocol using chlorine gas plasma was selected. Etch time ranged from 15 to 60 s for an etch rate of about 100 nm/min. The plasma intensity was static for the time period of etch and reached a pressure of 5×10^{-6} Torr when finished. The photoresist was removed completely by immersing in acetone and followed by piranha clean. The wafer was rinsed in DI water and dried under nitrogen. Metal films on Si-wafer substrates were then baked in air at 250 °C overnight for thermal oxidation of Ti to have a conformal oxide layer of TiO_2 on the patterned surface.

2.2.3. Deposition Of Amorphous Silica-Based Overlays Using PECVD. Plasma enhanced chemical vapor deposition (Oxford Plasmalab Systems 100 PECVD) of amorphous silica-based overlays was carried out in three steps. First, a conditioning step was used to prepare the chamber for the chemistries being used for the following deposition step. Next, the deposition of the desired chemistry was overlaid onto the wafer surface. Finally, a cleaning step was employed to prepare the PECVD system for future runs. For deposition, silane (SiH_4) was used as the Si source, N_2O was used as the oxygen source, and N_2/NH_3 was used as a precursor for nitrogen (N). The N incorporation in the $Si(ON)_x$ overlay is controlled by varying the relative flow rates of N_2O and N_2/NH_3. Higher flow rates of N_2 and

DOI: 10.1021/acsami.5b03319
ACS Appl. Mater. Interfaces 2015, 7, 15368−15379

NH_3 as compared to N_2O give a higher N/O ratio in the overlaid film. A standard protocol for SiO_x and SiN_x deposition from the Oxford PECVD system was initially selected. To vary the O/N ratio in the film, the N_2O, N_2, and NH_3 flow rates were adjusted. The optimized settings result in a lower deposition rate (64 nm/min) but conformal and higher quality films. Therefore, deposition would run approximately 90 s for a film thickness of about 100 nm. Deposition temperature was maintained at 350 °C throughout the deposition process. Pressure was maintained at 900 mTorr. Radio frequency power was maintained at 20−60 W. PECVD of Si−O−N films is tunable for film stress by use of dual (low and high) radio frequency for plasma excitation.[12] Plain samples (no patterns) with amorphous silica-based overlays were also fabricated for chemical and mechanical characterization of the overlays and for their use as control surfaces to study the impact of surface topography on cell behavior.

2.3. In-Process Thin Film Characterization. Characterization of samples during fabrication process was carried out at the CNMS facility at Oak Ridge National Laboratory (ORNL). These facilities were used to confirm and assess device structural, chemical, and mechanical properties as sample devices were fabricated. A spectroscopic ellipsometer (JA Woollam M-2000U) was used to determine the thickness and refractive index (denoted by n) of PECVD multilayered structures. An optical microscope (Leica DM4500P) was used for bright field transmission or reflected analysis of in-process samples to determine surface cleanliness between process steps and etch conformality and artifacts from etching processes. Film stress analysis was performed using the FSM 128 film stress measurement system (Frontier Semiconductor). A Veeco optical profilometer was used to measure etch depth before and after etch process steps.

After samples were prepared, a standard dicing saw was used to make 1 cm × 1 cm sections for postprocess characterization and *in vitro* testing.

2.4. Scanning Electron Microscopy (SEM). SEM analysis was conducted using two different SEM machines. For in-process characterization during sample fabrication, an SEM with capability of loading 4-in. wafer samples was desired so FEI Novalab 600 dual-beam (electron/ion) system at ORNL was used for in-process imaging/analysis. For postprocess characterization and *in vitro* testing, a JEOL 6010LA SEM was used to examine the small section samples. Both the SEMs were operated at 5−15 kV energy to get the finest results.

2.5. Transmission Electron Microscopy. TEM facilities were provided through the SHARE program in the High Temperature Materials Laboratory (HTML) at ORNL. Samples after fabrication were sectioned using a Hitachi NB5000 dual-beam scanning electron microscope focused ion beam (SEM-FIB) onto Cu grids prior to imaging by TEM. TEM imaging was carried out using a Hitachi HF-3300 300 kV FEG TEM/STEM with electron energy loss spectroscopy (EELS) for *in situ* X-ray diffraction analysis.

2.6. X-ray Photoelectron Spectroscopy (XPS). XPS facilities were also provided through the SHARE program at the HTML at ORNL. XPS analysis was conducted using a Thermo Scientific K-Alpha XPS with capabilities for sample through-thickness milling. This type of analysis can aid in getting surface and interfacial elemental chemical characterization.

2.7. Nanoscratch Testing. Adhesion of the PECVD-based amorphous silica overlays with the underlying metal/metal-oxide was determined through a nanomechanical scratch test on the sample surface. The adhesion/miscibility of overlays with Ti/TiO_2 was gauged by evaluating the friction/wear of the interfacial layers. An incremental load of (0−5000 μN) was applied to make a 10 μm long horizontal scratch on the sample surface using a cube-corner tip with the nanoindenter (Hysitron Ubi1 Nano-Indenter), and the change in resistance offered by interfacial layers as the tip goes deeper and deeper with increasing load was used to gauge the adhesion strength of the film.

2.8. X-ray Absorbance Near Edge Structure (XANES) Spectroscopy. XANES spectroscopy was conducted at the Canadian Light Source on the University of Saskatchewan in Saskatoon, Saskatchewan, Canada. XANES is an extremely useful and advanced tool to study partially crystalline or amorphous phases of bioceramics and investigate the local coordination of atoms and find their valence states.[34,35] The traditional characterization techniques (XRD, neutron diffraction, EDS) face challenges to analyze nanometer sized crystalline particles or partially crystallized structure of materials.[35] Therefore, XANES was employed to investigate the initial few nanometers layer of HCA. The phosphorus (P) L-edge spectra were probed using the Plane Grating Monochromator (PGM) beamline over the energy range 130−155 eV. PGM operates at the low-energy range between 5 and 250 eV, with a step size of 0.1 eV and shutter opening of 50 μm × 50 μm. The calcium (Ca) L-edge and oxygen (O) K-edge were characterized by the Spherical Grating Monochromator (SGM) beamline that operates in the midrange energy 250−2000 eV with a step size of 0.15 eV and shutter opening of 100 μm × 100 μm. The Ca L-edge and O K-edge spectra were recorded for energy ranges between 340 and 360 eV and 525 and 560 eV, respectively. The spectra for all samples were acquired after exposure to *in vitro* immersion for 6 h.

2.9. *In Vitro* Testing. *In vitro* testing was accomplished by immersing sample devices in cell culture medium (alpha-Minimum Essential Medium, α-MEM, Invitrogen Inc., Carlsbad, CA). Samples were placed into 6-well plates and immersed in 2 mL of media. Glass coverslips were used as an insoluble control samples for these experiments. Immersion testing was studied over several days, and samples were removed to determine various dissolution effects of *in vitro* conditions on surface properties. Immersion studies were conducted under ambient pressure and 37 °C at 100% relative humidity using a standard incubator.

2.10. Cell Culture Study. Human periosteal cells were used as an osteoblast progenitor. These cells were isolated from periosteum of femoral bone as described previously.[36] These cells differentiate into osteoblasts and express various osteogenic markers that include bone morphogenetic protein 2 (BMP2), lysyl oxidase (LOX), and osterix (OSX) when cultured in osteogenic media consisting of 50 ppm ascorbic acid, 1% penicillin−streptomycin, and 10% fetal bovine serum supplemented to α-MEM. They also form collagenous matrices and mineralized nodules when incubated for longer time *in vitro*.

The cells were cultured with growth media (1% penicillin−streptomycin and 10% fetal bovine serum supplemented to α-MEM) and were incubated at 37 °C. Once confluent, the cells were enzymatically dissociated with trypsin (0.25%)−EDTA (0.03%) solution for the experiments. The cells were seeded (50 000 cells per cm^2) onto control and test sample surfaces after prior 150 cm^2 flask cultures and expansion. The passage number of cells was maintained between 1 and 4 for all experiments. To determine the effect of sample surfaces on cells, gene expression studies were conducted. The samples were also tested for their long-term effect on collagen matrix formation and mineralized tissue analysis.

2.11. Gene-Expression Analysis. Quantitative reverse transcriptase polymerase chain reaction (qRT-PCR) was used to quantify levels of gene expression.[20] Cells were cultured on the test samples and the control surfaces for 3 days. The cells were lysed to extract the total RNA using the RNeasy Mini Kit (Qiagen, Valencia, CA). The extracts were transformed to cDNA using reverse transcriptase (Reverse Transcription System, Promega, Madison, WI) as per manufacturer's procedural guidelines. A full-spectrum UV−vis nanodrop volume analyzer (ND-1000, Nanodrop Technologies, Wilmington, DE) was used to quantify the total RNA and the converted cDNA for each sample. Absorbance measurements of total RNA or total cDNA concentrations were performed at 260 nm (A260) while A260/280 was used to estimate the purity of nucleic acids. All the cDNA samples (including controls) were diluted to a matching concentration of 100 ng/μL.

The samples were examined for three different types of osteogenic genes (BMP2, LOX, OSX) using an internal housekeeping gene (glyceraldehyde 3-phosphate dehydrogenase, GAPDH) for relative quantification. To quantify PCR, 10 μL reaction was performed for all samples. For this, 1 μL of cDNA solution was mixed with 5 μL of FastStart Taqman Probe Master (Roche Applied Sciences, Mannheim, Germany), 0.5 μL of gene template, and 3.5 μL of PCR grade water

DOI: 10.1021/acsami.5b03319
ACS Appl. Mater. Interfaces 2015, 7, 15368−15379

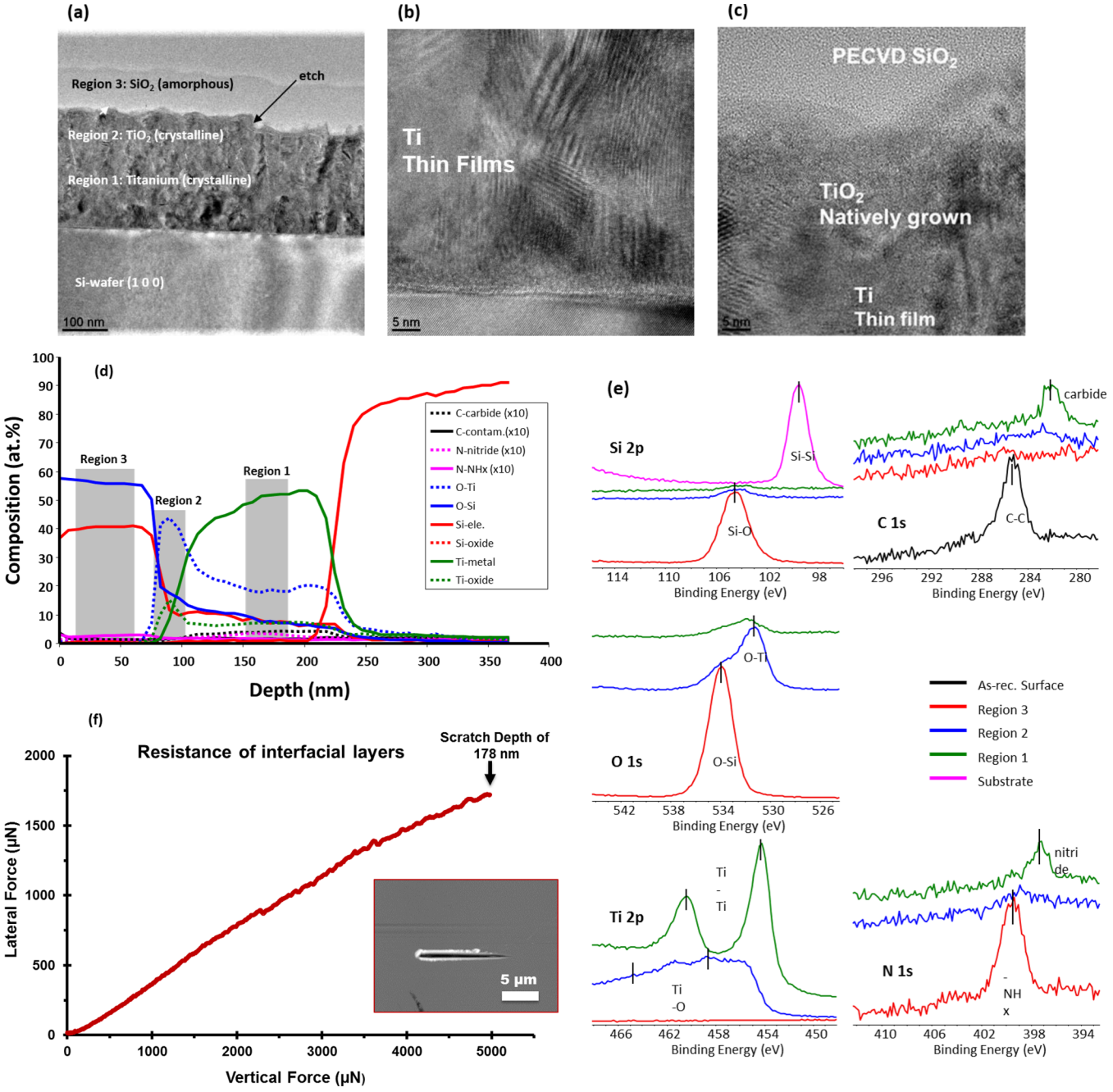

Figure 2. Characterization of nanofabricated devices. TEM micrographs (a–c) show lateral views of overlaid thin films. (a) The overall device consists of the PECVD SiO_x layer (region 3) deposited onto a natively grown TiO_2 layer (region 2), which was grown on an EB-PVD Ti layer (region 1). TEM micrograph at higher magnification shows (b) nanostructural features of EB-PVD Ti film and (c) adequate miscibility/adhesion between Ti–TiO_2–SiO_x interfacial layers. (d) X-ray photoelectron spectroscopy (XPS) analysis of through-thickness XPS data shows steadily diffused and chemically bonded interface composition whereas (e) surface and interfacial XPS data reveals surface elemental composition with corresponding binding energies of PECVD layers using different color lines. (f) Nanoscratch data exhibits no change in resistance with increasing vertical load that confirmed strong interfacial adhesion of SiO_x overlays with the underlying Ti-TiO_2 substrate. The inset shows the scanning probe micrograph of the surface after the incremental load (0–5000 μN) scratch test was done. The max depth of the scratch was 178 nm.

(Amgen Inc., South San Francisco, CA). Sample reaction was executed using a real-time PCR machine (ABI7500, Applied Biosystems Inc., Foster City, CA). Adequate plateau of the amplification ensured reliable threshold cycle (C_T) values, which were used to quantify relative gene expression using delta–delta C_T (Δ–Δ-C_T) method.

2.12. Raman Spectroscopy. Raman spectroscopy is a powerful technique to study biological samples like cells without involving lengthy procedures or the need for cell lysis, staining, or fixation, but it requires a relatively high-power laser beam to overcome the inherent low Raman scattering efficiency of biological molecules.[37,38] Microspot Raman spectroscopy (DXR, Thermo Scientific) was used to map dehydrated samples after *in vitro* cell cultures on the sample surface for 28 days to study the impact of surface chemistry on mineral deposition.[11] The spectroscope was operated at the following conditions: 780 nm laser source, 150 mW power, 50 μm slit, 10 Å objective, 10 s exposure. There were 32 spectra per location recorded between 400 and 2200 cm^{-1}. The presence of the carbonate (1072 cm^{-1}), phosphate (960 cm^{-1}), and hydroxyproline (876 cm^{-1}) bands of each averaged spectra was then recorded to compare mineral

DOI: 10.1021/acsami.5b03319
ACS Appl. Mater. Interfaces 2015, 7, 15368–15379

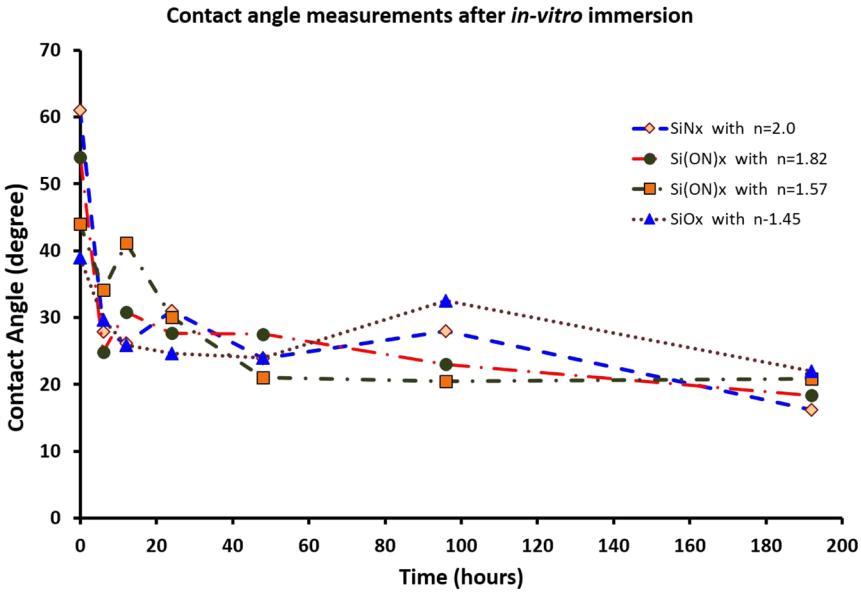

Figure 3. Contact angle measurements. PECVD-based SiO_x, $Si(ON)_x$, and SiN_x surfaces after *in vitro* immersion indicated hydrophilic functional group inductions in surface properties when immersed *in vitro*.

development in response to the surface effects of the test samples when compared to control samples.

3. STATISTICS

For *in vitro* experiments, triplicate samplings with duplicate experiments were conducted for all experiments. Analysis of variance was used for statistical analysis with $p < 0.05$ to determine statistical significance. For quantitative data taken on multiple samples of fabricated materials, error was nominally less than 1% and was therefore not reported.

4. RESULTS

4.1. Device Fabrication and Characterization. The TEM micrographs of the fabricated device used in this work are shown in Figure 2. The image shows three regions fabricated on top of the Si-wafer substrate. Region 1 is the EB-PVD Ti layer, region 2 is the thermally grown TiO_2 layer, and region 3 is the PECVD-based SiO_x layer. Ti layers were observed to have a columnar structure with an average column width of about 100 nm, indicating line-of-sight deposition. Characterization using EELS analysis indicated the presence of anatase Ti (result not shown). Within the Ti layer, aligned columnar atom planes of Ti were observed, which indicates that the columnar microstructures were composed of these oriented atom planes (Figure 2b).

At the top of the Ti layer, etching showed distinct etched regions spaced 2 μm apart from each other. Sidewalls exhibited some curvature indicating a certain isotropy of the etch profile using cryogenic chlorine gas. An induction period of 15 s was observed, and a steady postinduction etch rate of about 100 nm/min was recorded for all the samples. Within a sample, the etch depth for all etched trenches was found to be highly uniform.

The natively grown TiO_2 was overlaid with a PECVD silica layer. PECVD overlays were found to be contoured with the underlying etched surface; however, some rounding of sidewalls did occur. The interface between the PECVD overlay and underlying Ti/TiO_2 was observed to have a gradual transition with microstructural features distinct for each region and a less distinctive microstructure between regions (Figure 2c).

Results from XPS analysis (Figure 2d) were obtained by milling through the thickness of the device. The data showed elemental composition from the surface of PECVD silica (region 3, Figure 2a) to the Si-wafer substrate. The XPS results confirmed the overlay thickness of PECVD SiO_x to be approximately 100 nm, with 300 nm of Ti layer, and a graded interface between the SiO_x overlay and TiO_2 layers. This graded interface shows that atomic % composition of oxygen is nearly 2 times higher than that of Si or Ti at the interface. It means that, for every Si atom, there are 2 oxygen atoms, and likewise every Ti atom is bonded to 2 oxygen atoms that represents a nearly stoichiometric SiO_2-TiO_2 interface, indicating that the silica and titania layers formed ionic bonding between the two layers. The TiO_2 layer was distinct and had a thickness of approximately 10 nm; however, data for oxygen diffusion within the Ti layer (O−Ti) showed some oxygen diffused into the Ti layer. This is likely due to O diffusion along the columnar grain boundaries.[39] Potential contamination of N and C during PECVD was insignificant due to the additional air plasma-cleaning step in our fabrication process. Without plasma-cleaning, N and C can be as high as 10 and 14 at. %, respectively.[40] Nanoscratch testing showed no significant change in resistance when we scratch through the SiO_2-TiO_2-Ti interface, which indicated adequate miscibility of the interfacial layers (Figure 2f).

4.2. In Vitro Testing of Nanofabricated Devices. Cell-free *in vitro* testing was conducted to determine the effect of *in vitro* conditions on PECVD silica surfaces. In this study, nitrogen was incorporated into amorphous silica overlays to determine the effect on N substitution of O on surface chemistry during *in vitro* immersion. Ti layers were not used to isolate the effect of *in vitro* conditions on amorphous silica-based material chemistry when compared to control glass surfaces.

The effects of *in vitro* conditions on SiO_x, $Si(ON)_x$, and SiN_x surface contact angles are demonstrated in Figure 3. Initially, SiO_x layers had a lower contact angle, indicating their initial

DOI: 10.1021/acsami.5b03319
ACS Appl. Mater. Interfaces 2015, 7, 15368−15379

relative hydrophilicity. On the other hand, the SiN_x layers exhibited a relatively high contact angle and indicated their relative hydrophobicity. After a few hours, the contact angle decreased for all samples and was approximately the same after 24 h. This change in contact angle with time indicated that these surfaces experienced hydrophilic functional group changes during *in vitro* immersion.

The results from the XANES data were analyzed to illustrate the effect of *in vitro* conditions on surface elements present on the PECVD SiO_x, $Si(ON)_x$, and SiN_x overlays. XANES data (Figure 4) showed that, after 6 h of *in vitro* immersion, Ca was present in relatively large abundance on the surface of all tested materials. XANES data analysis confirmed the presence of P species on all surfaces as well (Figure 4b). However, the presence of noise in the peaks for samples with high N content (n = 2.0, n = 1.82) indicated that these surfaces had a relatively smaller amount of phosphate, which was not sufficient to give enough of a signal-to-noise ratio. But samples with relatively lower N content clearly showed plentiful phosphates present on the surface, indicated by the characteristic peak for phosphate at around 148 eV energy.

Although all materials tested showed the presence of Ca-phosphate species that were found in relatively smaller quantity for samples with higher N/O ratio in the overlay, an interesting trend was observed when the coordination of O was analyzed on these surfaces (Figure 4c). The results of XANES data on the coordination of oxygen revealed that O coordination exhibited a pattern indicating the presence of hydroxycarbonate apatite. The characteristic peaks for pure HA are the pre-edge peak at around 536 eV, strong peak at around 539 eV, and the shoulder at around 545 eV (shown by the model compounds spectra on left side in Figure 4c). As the N content increased (and thus substituting for O), the presence of O peaks coordinated in a carbonate structure appeared with increasing intensity relative to the peak showing O coordinated into a phosphate structure. In other words, samples with less N content (n = 1.45, n = 1.57) showed Ca-phosphates but not enough carbonate formation whereas higher N content samples (n = 1.82, n = 2.0) evidently showed carbonate-substituted calcium phosphate (known as hydroxycarbonate apatite, HCA), identified by a carbonate characteristic peak at around 535 eV. This coupled formation of carbonate and phosphate near edge structures indicates the presence of hydroxycarbonate apatite with increasing carbonate to phosphate ratio as the N/O ratio increased in the overlay.

4.3. Cell Cultures Studies of Nanofabricated Devices.

These materials were also tested for osteogenic properties *in vitro* using human periosteal cells. Gene expression of osteoblast markers, extracellular matrix collagen production, and mineralized nodule formation were studied. Cells were cultured for 3 days to determine the effect of surfaces on gene expression, 6 days for ECM collagen formation, and 4 weeks for mineralized nodule formation. Figure 5 shows the results for relative expression of osteogenic gene markers. All surfaces were observed to enhance BMP2 and OSX expression to levels 2−4-fold higher than control surfaces. However, maximal enhancement of these markers occurred on $Si(ON)_x$ surfaces. All the samples were statistically different from each other with a p-value of $p < 0.05$ (ANOVA).

The results for ECM collagen formation on sample surfaces after *in vitro* cell seeding are shown in Figure 6. SiO_x surfaces facilitated the migration of cells over their surfaces on the textured area. SiN_x surfaces were observed to have cells remain

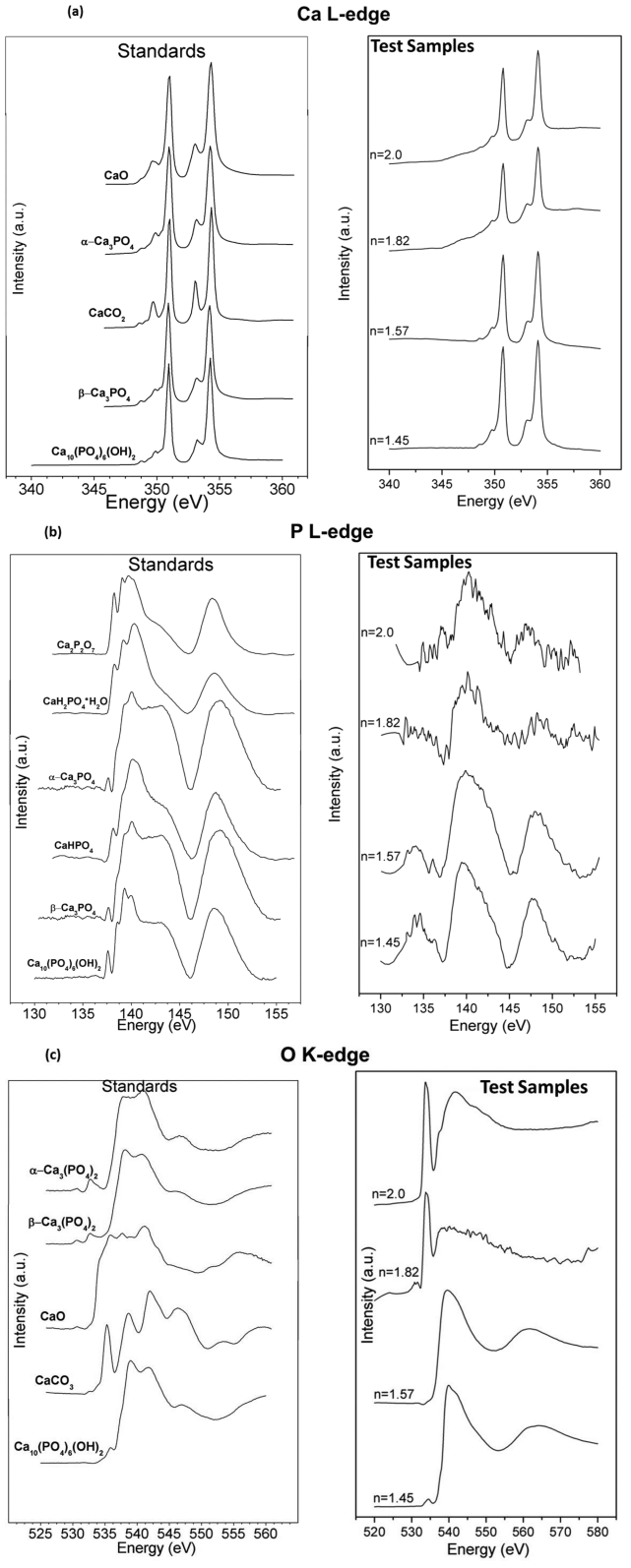

Figure 4. X-ray absorbance near edge structure (XANES) spectroscopy. Comparative data for (L) standards and (R) PECVD-based SiO_x (n = 1.45), $Si(ON)_x$ (n = 1.57, n = 1.82), and SiN_x (n = 2.0) samples where "n" represents the refractive index for the characteristic surface. Test samples were investigated after 6 h of *in vitro* immersion to examine the presence of (a) calcium, (b) phosphorus, and (c) oxygen on the surface of each sample. The data analysis reveals the formation of hydroxycarbonate apatite with higher carbonate to phosphate ratio as the N/O ratio increases in the overlay.

DOI: 10.1021/acsami.5b03319
ACS Appl. Mater. Interfaces 2015, 7, 15368−15379

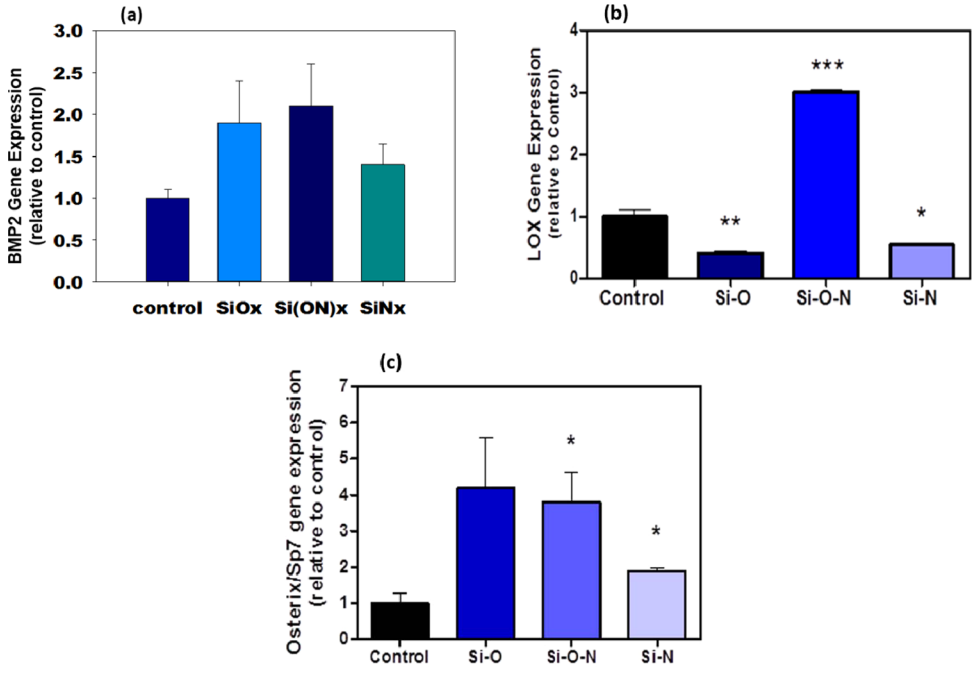

Figure 5. Human periosteal cell osteogenic gene expression data for (a) BMP2, (b) LOX, and (c) OSX after 3 days in culture shows many-fold enhanced expression of these osteogenic markers (ANOVA, * indicates statistical significance, $p < 0.05$).

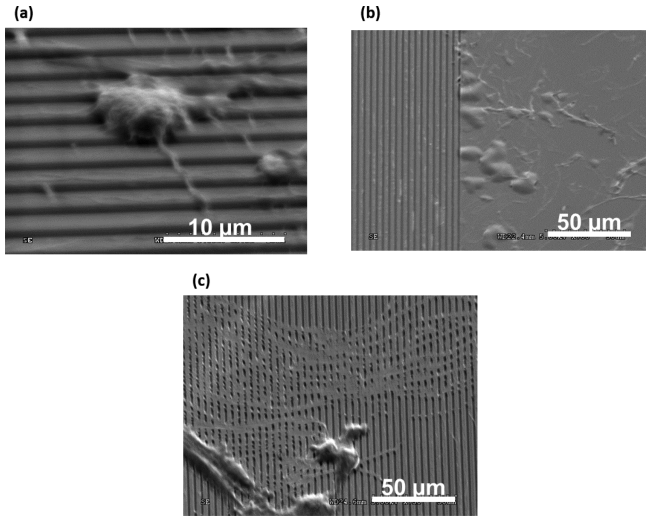

Figure 6. SEM micrographs compare extracellular matrix (ECM) collagen production by human periosteal cells after 6 days in culture for (a) SiO_x, (b) $Si(ON)_x$, and (c) SiN_x overlays.

on the flat section of their surfaces. In both cases, the formation of "collagen-like" ECM formation was not observed. On $Si(ON)_x$ surface, though, cells were observed to form collagenous matrices, indicated by the orthogonal arrangement of the formed ECM with the surface texture orientation. Raman spectroscopy showed amide I, amide III, and hydroxyproline peaks at a later stage (Figure 7), which confirmed the collagen formation on the $Si(ON)_x$ sample surface.

Figure 7 demonstrates the effect of $Si(ON)_x$ surface chemistry on biomineral development in comparison to control surfaces. Control surfaces were observed to have cell formation of collagenous ECM after 4 weeks; however, no presence of biomineral was observed. Similar effects were seen for SiO_x and SiN_x (results not shown). On the other hand, $Si(ON)_x$ surfaces were observed to form biomineral. This was evident by the formation of white nodules and the presence of both carbonate and phosphate functional groups on their surface. Taken together, $Si(ON)_x$ surfaces facilitated the formation of rapid biomineral formation through the maximal enhancement of osteogenic gene expression and early ECM collagen formation.

5. DISCUSSION

This study showed the effect that PECVD amorphous silica-based materials have on surface modification of Ti/TiO_2-based devices and osteoprogenitor response. PECVD-based SiO_x overlays were found to be very adherent to the stoichiometric Si−O−Ti interface between SiO_x and Ti/TiO_2. Nanoscratch results showed strong interfacial adhesion without delamination as the scratch testing progressed. Cell-free *in vitro* studies exhibited changes in contact angles over 24 h and changes in surface formation with the presence of carbonate apatite within a few hours of immersion. Understanding of apatite formation *in vitro* for bioactive silica-based materials and their dissolution has concentrated on bioactive glasses. Bioactive glasses undergo rapid ion exchange of alkali metal cations (group I: Na^+, K^+) and relatively slower exchange of alkaline earth metal cations (group II: Ca^{2+}, Mg^{2+}) with liquid protons to infiltrate the silica network. After this has occurred, surface silanols (evident by Si−OH Raman bond stretch) are available for dissolution, polymerization, and reprecipitation to form a silica gel network, which leads to apatite formation. Whereas PECVD-based silica forms surface silanols readily,[40] skipping the group I and group II ion exchange step. Studies show that low-temperature PECVD provides even more silanols on the oxide surface.[12] Thus, the PECVD process provides the surface silanols immediately available for dissolution, polymerization, and reprecipitation to form the silica gel network, resulting in apatite formation within 6 h of *in vitro* submersion. Cell culture testing showed the presence of collagen on all materials including control surfaces; however, $Si(ON)_x$ surfaces maximally enhanced periosteal cell osteogenic gene expression and

DOI: 10.1021/acsami.5b03319
ACS Appl. Mater. Interfaces 2015, 7, 15368−15379

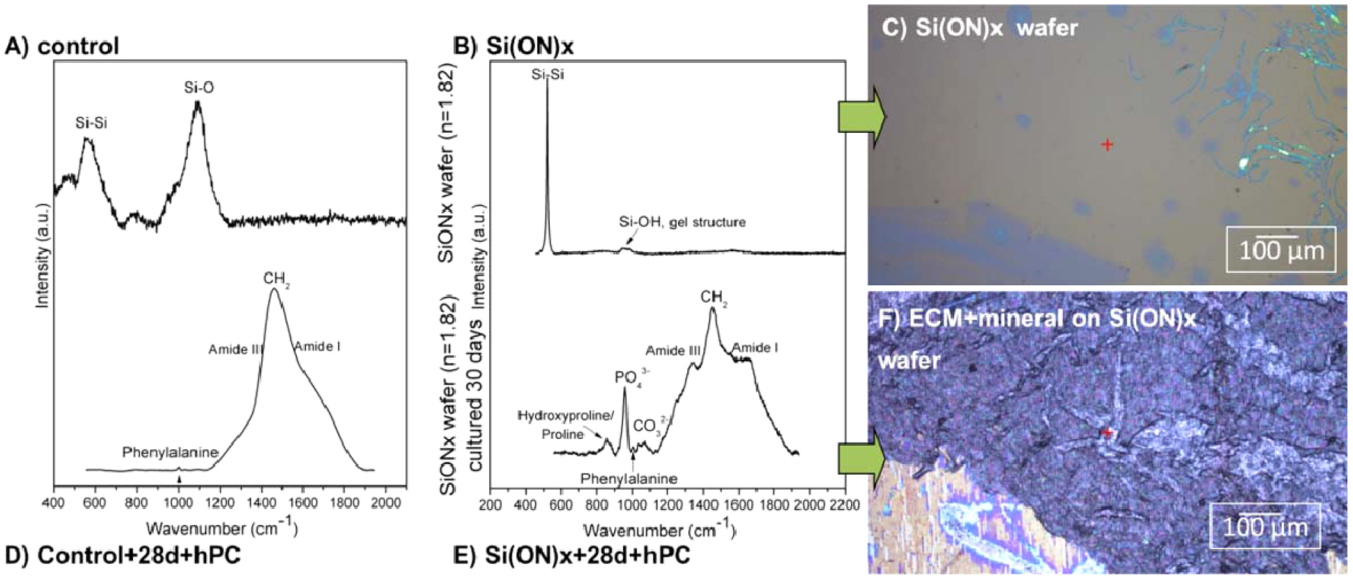

Figure 7. Analysis of ECM after 4 weeks of *in vitro* human periosteal cell culture. Raman spectroscopy showed initial layers of silica for (a) control and (b) $Si(ON)_x$ surfaces. (c) Similarly, the optical micrograph showed no minerals present on the surfaces initially. After 4 weeks of *in vitro* cell culture, biomineral development on the sample surfaces were compared. (d) Control surface showed accumulation of collagenous matrices only with no biomineral present whereas (e) $Si(ON)_x$ surfaces exhibited the formation of carbonate, phosphate, and amide peaks associated with mineralized tissue to indicate the presence of collagenous matrices. (f) Optical micrograph showed the presence of hydroxycarbonate apatite biomineral on the $Si(ON)_x$ surface, indicated by the formation of white nodules on the surface.

stimulated added production of carbonate apatite biomineral matrix. Therefore, these overlays support the hypothesis that they can provide structural support by exhibiting strong adhesion to the underlying Ti/TiO_2 layers and stimulate the rapid formation of bone-like biomineral formation.

The process flow used for these studies provides precise control over texture, surface chemistry, and surface mechanics that are exposed to cells and tissues. Optical lithography was employed due to its scalable features that can be fabricated at relatively low cost and with high reproducibility. Uses of cryogenic chlorine gas for metal etching resulted in an initial induction period before a linear period of etch depth with time. The lag time in the etch method was observed, and this was owed to an initial induction period to etch through a relatively small native oxide layer of TiO_2, which may allow etching ions to build on surface due to the highly capacitive nature of surface oxide. Etches were intended to be anisotropic; however, some degree of isotropy was observed. This was evident by the presence of angled sidewalls of etched trenches. This could be owed to the columnar grain structure of the EB-PVD Ti. Others have noted improved sidewall formation when using Ti wafers etched with cryogenic chlorine gas.[41] Another possible explanation for the somewhat isotropic etch was the possible lack of delivery of a sufficiently high-density low-pressure plasma column to create anisotropic etch.[42] Thermal annealing of Ti thin film yielded a TiO_2 layer that appeared tensile. The tensile nature of the stress was expected for low-temperature deposited TiO_2 film[43] and indicated that the film was not being constrained by the underlying Ti (likely owed to its columnar grain structure). Despite these relatively small issues with etching, overall control over grain structure and etching of Ti as well as growth of thermal TiO_2 was well-controlled and reproducible.

In this work, we evaluated the properties of the PECVD-based SiO_x-Ti/TiO_2 interface. The key advantage of this interface was the presence of a nearly stoichiometric Ti−O−Si bond. Several studies have indicated that the formation of this interface is owed to migration of Ti and Si atoms into each layer.[44−47] Nanoscratch results further confirmed that this interface does not delaminate and that the overlay is strongly adherent, which confirmed the result.[48] Moreover, because the overlay thickness is relatively small compared to the rest of the device, this offers additional benefit of high resistance to peel off stress, as suggested by Saiz and Tomsia.[24] In comparison, bulk methods used to fabricate bioactive glass or hydroxyapatite coatings on Ti/TiO_2 did not adhere well. This was mainly owed to relatively high deposition temperatures, thermal expansion mismatch, large coating thickness to interface thickness (1000:1 in the case of bioactive glass), or lack of miscibility with synthetic HA and Ti/TiO_2.[49] PECVD, on the other hand, can be more advantageous as a relatively low-temperature method to fabricate thin and well-adherent SiO_x-based overlays on Ti.

Such potential to improve fracture healing must come with an ability of the overlay materials to stimulate or enhance osteogenesis and "bone-like" biomineral formation. PECVD-based SiO_x overlay resulted in the formation of Ca-PO_4-based hydroxyapatite formation within 6 h. However, doping with N in $Si(ON)_x$ and SiN_x resulted in hydroxycarbonate apatite formation. This led to enhanced osteogenic expression of BMP2 and LOX, which are key markers of enhanced osteogenesis. Although SiO_x appeared to induce higher expression of OSX, it was not statistically significant, whereas $Si(ON)_x$ enhanced expression was significant relative to control levels. Still, $Si(ON)_x$ and SiO_x enhancement were not significant when compared with each other and appeared very close in average value; therefore, these levels of enhancement were deemed very similar. There is, however, a significant enhancement of LOX expression when periosteal cells are exposed to $Si(ON)_x$ surfaces. LOX is a key collagen cross-linking enzyme and is responsible for increasing biomineral strength.[50] Without enhancement of the cross-linking enzyme

DOI: 10.1021/acsami.5b03319
ACS Appl. Mater. Interfaces 2015, 7, 15368−15379

at the early phase of osteogenesis, biomineral formation can be delayed. This could explain the rapid enhancement in biomineral production on $Si(ON)_x$ surfaces. Interestingly, only the $Si(ON)_x$ layer induced the formation of biomineral of similar chemistry by human periosteal cells, whereas SiO_x and SiN_x did not. In addition, periosteal cells only had enhanced expression of LOX and deposited a collagenous ECM in orthogonally arranged structure to the patterned $Si(ON)_x$ surface, which is consistent with the formation of collagenous ECM by osteoprogenitor cells during the formation of bone matrix.[20] This may be owed to the human periosteal cells requiring the presence of carbonate and phosphate on the surface to produce bone-like HCA. These results are the first evidence showing this optimal effect of N doping in SiO_x to produce HCA within a few hours of *in vitro* immersion and resultant enhancements in osteogenesis and biomineral formation within 4 weeks.

In the Si−O−N elemental system, N acts as a substitute for O resulting in a higher atomic packing density. SiO_x and SiN_x maintain tetrahedral and trigonal coordination, respectively; $Si(ON)_x$ coordination has a mixture of these 2 coordination systems.[22] As N concentration increases in amorphous silica-based material, the mechanical strength increases significantly (Young's modulus rises from 73 to 166 GPa whereas hardness increases from 8.32 to 17.10 GPa).[22,51] Though annealed amorphous silica-based bioactive glass coatings on Ti and sputter coated oxynitride films on Si have both exhibited improved mechanical strength with increasing N content,[22,24] the role of N in biomineralization has never been explored or understood.

In this study, there is clear evidence that N influences the chemistry of biominerals such that carbonate can be incorporated. The only evidence of a similar effect is in the deep-sea sponges in which their siliceous skeletons have been shown to incorporate carbonate species in an environment with limited soluble oxygen.[52] It can be speculated that the altered glass network could provide surface site coordination more favorable to carbonate formation. However, no evidence has been shown that these deep-sea sponges incorporate N into their skeletons. It will be necessary to isolate the effect of N in biomineralization to gain a better understanding of how it impacts carbonate formation or to assess if this is an effect related to a paucity in oxygen content.

In terms of the intended application of these overlays for traumatic fracture healing, several studies still remain before they can be used for clinical applications. First, understanding of the mechanisms of these layers with upstream cellular responses must be determined so that better control over cellular response and biomineral formation can be achieved. Second, animal testing must be conducted to determine how these overlays perform in an environment where hormones and biomechanical loads are present. Finally, a better understanding of the mechanisms involving biomineral formation on each of these substrates is needed to uncover the role that N plays during apatite formation and biomineralization.

6. CONCLUSIONS

In this study, we showed that PECVD amorphous silica-based overlays exhibit strong adhesion to Ti/TiO_2-based devices and incorporation of N enhanced the osteogenesis of osteoprogenitor cells and biomineral formation. The SiO_x-TiO_2−Ti interface showed continuity in chemical composition from the overlying SiO_x layer to the TiO_2 layer and then onto the Ti layer. The interface exhibited strong adhesion between layers. *In vitro* testing showed that the incorporation of N induced the formation of increasing carbonate to phosphate ratio. The $Si(ON)_x$ layers induced osteogenesis of human periosteal cells and carbonate apatite biomineral matrix formation. In future, this study can potentially be used in clinical applications where surface features facilitate cellular response and biomechanical bonding while the surface chemistry augments biochemical bonding via early formation of hydroxycarbonate apatite to hasten bone matrix formation.

AUTHOR INFORMATION

Corresponding Author

*Phone: +1-214-370-7006. Fax: +1-214-874-4538. E-mail: varanasi@bcd.tamhsc.edu.

Notes

The authors declare no competing financial interest.

ACKNOWLEDGMENTS

The authors would like to thank Megen F. Velten for her valuable contributions to *in vitro* studies and analysis, Harry Meyer and Karren More for their help with nanofabricated surface characterization, and Vibhu Sharma for his assistance with nanoscratch testing. We also acknowledge the staff at the Center for Nanophase Material Science at the Oak Ridge National Laboratory and the Nanotechnology Research Center, University of Texas at Arlington, for their help and guidance on device fabrication and characterization. XANES experiments were conducted at the Canadian Light Source, Saskatoon, Canada, which is supported by NSERC, NRC, CIHR, and the University of Saskatchewan. The work was supported by a grant from National Institutes of Health (1R03DE023872-01A1) to V.G.V. and partially supported by Enhancement Grant (#24444100005, V.G.V., PI), Departmental Startup (#304-128170, V.G.V., PI), and CNMS Grant (#2010-080, V.G.V., PI).

REFERENCES

(1) Pitts, S. R.; Niska, R. W.; Xu, J.; Burt, C. W. National Hospital Ambulatory Medical Care Survey: 2006 Emergency Department Summary. *Natl. Health Stat. Rep.* **2008**, *7*, 1−38.

(2) Montjovent, M.-O.; Mathieu, L.; Hinz, B.; Applegate, L. L.; Bourban, P.-E.; Zambelli, P.-Y.; Månson, J.-A.; Pioletti, D. P. Biocompatibility of Bioresorbable Poly (L-Lactic Acid) Composite Scaffolds Obtained by Supercritical Gas Foaming with Human Fetal Bone Cells. *Tissue Eng.* **2005**, *11*, 1640−1649.

(3) Fabian, E.; Gerstorfer, I.; Thaler, H. W.; Stundner, H.; Biswas, P.; Elmadfa, I. Nutritional Supplementation Affects Postoperative Oxidative Stress and Duration of Hospitalization in Patients with Hip Fracture. *Wien. Klin. Wochenschr.* **2011**, *123*, 88−93.

(4) Sandukji, A.; Al-Sawaf, H.; Mohamadin, A.; Alrashidi, Y.; Sheweita, S. A. Oxidative Stress and Bone Markers in Plasma of Patients with Long-Bone Fixative Surgery: Role of Antioxidants. *Hum. Exp. Toxicol.* **2011**, *30*, 435−42.

(5) Hannemann, A.; Friedrich1, N.; Spielhagen, C.; Rettig, R.; Ittermann, T.; Nauck, M.; Wallaschofski, H. Reference Intervals for Serum Osteocalcin Concentrations in Adult Men and Women from the Study of Health in Pomerania. *BMC Endocr. Disord.* **2013**, *13*, 11.

(6) Tousi, N. S.; Velten, M. F.; Bishop, T. J.; Leong, K. K.; Barkhordar, N. S.; Marshall, G. W.; Loomer, P. M.; Aswath, P. B.; Varanasi, V. G. Combinatorial Effect of Si4+, Ca2+, and Mg2+ Released from Bioactive Glasses on Osteoblast Osteocalcin Expression and Biomineralization. *Mater. Sci. Eng., C* **2013**, *33*, 2757−2765.

(7) Canullo, L.; Dellavia, C. Sinus Lift Using a Nanocrystalline Hydroxyapatite Silica Gel in Severely Resorbed Maxillae: Histological

DOI: 10.1021/acsami.5b03319
ACS Appl. Mater. Interfaces 2015, 7, 15368−15379

Preliminary Study. *Clin. Implant Dent. Relat. Res.* **2009**, *11* (Suppl 1), E7−13.
(8) Banwart, Jc; Asher, Ma; Hassanein, Rs. Iliac Crest Bone Graft Harvest Donor Site Morbidity. A Statistical Evaluation. *Spine (Philadelphia)* **1995**, *20*, 1055−60.
(9) Iwai-Yoshida, M.; Shibata, Y.; Suzuki, D.; Fujisawa, N.; Tanimoto, Y.; Kamijo, R.; Maki, K.; Miyazaki, T. Antioxidant and Osteogenic Properties of Anodically Oxidized Titanium. *J. Mech. Behav. Biomed. Mater.* **2012**, *13*, 230−236.
(10) Foppiano, S.; Marshall, S. J.; Marshall, G. W.; Saiz, E.; Tomsia, A. P. Bioactive Glass Coatings Affect the Behavior of Osteoblast-Like Cells. *Acta Biomater.* **2007**, *3*, 765−771.
(11) Tousi, N. S.; Velten, M. F.; Bishop, T. J.; Leong, K. K.; Barkhordar, N. S.; Marshall, G. W.; Loomer, P. M.; Aswath, P. B.; Varanasi, V. G. Combinatorial Effect of Si 4+, Ca 2+, and Mg 2+ Released from Bioactive Glasses on Osteoblast Osteocalcin Expression and Biomineralization. *Mater. Sci. Eng., C* **2013**, *33*, 2757−2765.
(12) Ceiler, M.; Kohl, P.; Bidstrup, S. Plasma-Enhanced Chemical Vapor Deposition of Silicon Dioxide Deposited at Low Temperatures. *J. Electrochem. Soc.* **1995**, *142*, 2067−2071.
(13) Cverna, F. *Thermal Properties of Metals*; ASM International: Materials Park, OH, 2002.
(14) Diebold, U. The Surface Science of Titanium Dioxide. *Surf. Sci. Rep.* **2003**, *48*, 53−229.
(15) Lopez-Esteban, S.; Saiz, E.; Fujino, S.; Oku, T.; Suganuma, K.; Tomsia, A. P. Bioactive Glass Coatings for Orthopedic Metallic Implants. *J. Eur. Ceram. Soc.* **2003**, *23*, 2921−2930.
(16) Gomez-Vega, J.; Saiz, E.; Tomsia, A.; Marshall, G.; Marshall, S. Bioactive Glass Coatings with Hydroxyapatite and Bioglass Particles on Ti-Based Implants. 1. Processing. *Biomaterials* **2000**, *21*, 105−111.
(17) Kobayashi J.; Goetz, W. K. Growth of III-Nitride Films on Mismatched Substrates without Conventional Low Temperature Nucleation Layers. U.S. Patent 6900067 A2, 2005.
(18) Varanasi, V. G.; Besmann, T. M.; Anderson, T. J. Equilibrium Analysis of Cvd of Yttria-Stabilized Zirconia. *J. Electrochem. Soc.* **2005**, *152*, C7−C14.
(19) Varanasi, V. G.; Besmann, T. M.; Payzant, E. A.; Pint, B. A.; Lothian, J. L.; Anderson, T. J. High-Growth Rate Ysz Thermal Barrier Coatings Deposited by Mocvd Demonstrate High Thermal Cycling Lifetime. *Mater. Sci. Eng., A* **2011**, *528*, 978−985.
(20) Varanasi, V.; Saiz, E.; Loomer, P.; Ancheta, B.; Uritani, N.; Ho, S.; Tomsia, A.; Marshall, S.; Marshall, G. Enhanced Osteocalcin Expression by Osteoblast-Like Cells (Mc3t3-E1) Exposed to Bioactive Coating Glass (Sio 2−Cao−P 2 O 5−Mgo−K 2 O−Na 2 O System) Ions. *Acta Biomater.* **2009**, *5*, 3536−3547.
(21) Varanasi, V. G.; Besmann, T. M.; Payzant, E. A.; Starr, T.; Anderson, T. Thermodynamic Analysis and Growth of Zro 2 by Chloride Chemical Vapor Deposition. *Thin Solid Films* **2008**, *516*, 6133−6139.
(22) Liu, Y.; Lin, I.-K.; Zhang, X. Mechanical Properties of Sputtered Silicon Oxynitride Films by Nanoindentation. *Mater. Sci. Eng., A* **2008**, *489*, 294−301.
(23) Bachar, A.; Mercier, C.; Tricoteaux, A.; Hampshire, S.; Leriche, A.; Follet, C. Effect of Nitrogen and Fluorine on Mechanical Properties and Bioactivity in Two Series of Bioactive Glasses. *J. Mech. Behav. Biomed. Mater.* **2013**, *23*, 133−148.
(24) Gomez-Vega, J.; Saiz, E.; Tomsia, A. Glass-Based Coatings for Titanium Implant Alloys. *J. Biomed. Mater. Res.* **1999**, *46*, 549−559.
(25) Jeon, H.; Simon, C. G.; Kim, G. A Mini-Review: Cell Response to Microscale, Nanoscale, and Hierarchical Patterning of Surface Structure. *J. Biomed. Mater. Res., Part B* **2014**, *102*, 1580−1594.
(26) Seunarine, K.; Curtis, A. S.; Meredith, D.; Wilkinson, C. D.; Riehle, M.; Gadegaard, N. A Hierarchical Response of Cells to Perpendicular Micro-and Nanometric Textural Cues. *IEEE Trans. NanoBiosci.* **2009**, *8*, 219−225.
(27) Asghar, W.; Kim, Y.-T.; Ilyas, A.; Sankaran, J.; Wan, Y.; Iqbal, S. M. Synthesis of Nano-Textured Biocompatible Scaffolds from Chicken Eggshells. *Nanotechnology* **2012**, *23*, 475601.
(28) Albrektsson, T.; Wennerberg, A. Oral Implant Surfaces: Part 1—Review Focusing on Topographic and Chemical Properties of Different Surfaces and in Vivo Responses to Them. *Int. J. Prosthodontics* **2003**, *17*, 536−543.
(29) Van Raay, J.; Rozing, P.; Van Blitterswijk, C.; Van Haastert, R.; Koerten, H. Biocompatibility of Wear-Resistant Coatings in Orthopaedic Surgery in Vitro Testing with Human Fibroblast Cell Cultures. *J. Mater. Sci.: Mater. Med.* **1995**, *6*, 80−84.
(30) De Giglio, E.; Sabbatini, L.; Colucci, S.; Zambonin, G. Synthesis, Analytical Characterization, and Osteoblast Adhesion Properties on Rgd-Grafted Polypyrrole Coatings on Titanium Substrates. *J. Biomater. Sci., Polym. Ed.* **2000**, *11*, 1073−1083.
(31) Schroeder, A.; Francz, G.; Bruinink, A.; Hauert, R.; Mayer, J.; Wintermantel, E. Titanium Containing Amorphous Hydrogenated Carbon Films (Ac: H/Ti): Surface Analysis and Evaluation of Cellular Reactions Using Bone Marrow Cell Cultures in Vitro. *Biomaterials* **2000**, *21*, 449−456.
(32) Hamlet, S.; Alfarsi, M.; George, R.; Ivanovski, S. The Effect of Hydrophilic Titanium Surface Modification on Macrophage Inflammatory Cytokine Gene Expression. *Clin. Oral Implants Res.* **2012**, *23*, 584−590.
(33) Odatsu, T.; Azimaie, T.; Velten, M. F.; Vu, M.; Lyles, M. B.; Kim, H. S.; Aswath, P. B.; Varanasi, V. G. Human Periosteum Cell Osteogenic Differentiation Enhanced by Ionic Silicon Release from Porous Amorphous Silica Fibrous Scaffolds. *J. Biomed. Mater. Res., Part A* **2015**, DOI: 10.1002/jbm.a.35412.
(34) Demirkiran, H.; Hu, Y.; Zuin, L.; Appathurai, N.; Aswath, P. B. Xanes Analysis of Calcium and Sodium Phosphates and Silicates and Hydroxyapatite−Bioglass® 45s5 Co-Sintered Bioceramics. *Mater. Sci. Eng., C* **2011**, *31*, 134−143.
(35) Rajendran, J.; Gialanella, S.; Aswath, P. B. Xanes Analysis of Dried and Calcined Bones. *Mater. Sci. Eng., C* **2013**, *33*, 3968−3979.
(36) Kim, H. K. W.; Oxendine, I.; Kamiya, N. High-Concentration of Bmp2 Reduces Cell Proliferation and Increases Apoptosis Via Dkk1 and Sost in Human Primary Periosteal Cells. *Bone* **2013**, *54*, 141−150.
(37) Notingher, I.; Jell, G.; Notingher, P. L.; Bisson, I.; Tsigkou, O.; Polak, J. M.; Stevens, M. M.; Hench, L. L. Multivariate Analysis of Raman Spectra for in Vitro Non-Invasive Studies of Living Cells. *J. Mol. Struct.* **2005**, *744*, 179−185.
(38) Puppels, G.; De Mul, F.; Otto, C.; Greve, J.; Robert-Nicoud, M.; Arndt-Jovin, D.; Jovin, T. Studying Single Living Cells and Chromosomes by Confocal Raman Microspectroscopy. *Nature* **1990**, *347*, 301−303.
(39) Golightly, F.; Stott, F.; Wood, G. The Influence of Yttrium Additions on the Oxide-Scale Adhesion to an Iron-Chromium-Aluminum Alloy. *Oxid. Met.* **1976**, *10*, 163−187.
(40) Szili, E. J.; Kumar, S.; Smart, R. S. C.; Lowe, R.; Saiz, E.; Voelcker, N. H. Plasma Enhanced Chemical Vapour Deposition of Silica onto Titanium: Analysis of Surface Chemistry, Morphology and Hydroxylation. *Surf. Sci.* **2008**, *602*, 2402−2411.
(41) Domanski, M.; Luttge, R.; Lamers, E.; Walboomers, X.; Winnubst, L.; Jansen, J.; Gardeniers, J. Submicron-Patterning of Bulk Titanium by Nanoimprint Lithography and Reactive Ion Etching. *Nanotechnology* **2012**, *23*, 065306.
(42) McAuley, S.; Ashraf, H.; Atabo, L.; Chambers, A.; Hall, S.; Hopkins, J.; Nicholls, G. Silicon Micromachining Using a High-Density Plasma Source. *J. Phys. D: Appl. Phys.* **2001**, *34*, 2769.
(43) Burgos, M.; Langlet, M. Condensation and Densification Mechanism of Sol-Gel Tio2 Layers at Low Temperature. *J. Sol-Gel Sci. Technol.* **1999**, *16*, 267−276.
(44) Dunn, D.; Hull, R.; Ross, F.; Tromp, R. Texture Transformations in Reactive Metal Films Deposited Upon Amorphous Substrates. *J. Appl. Phys.* **2001**, *89*, 2635−2640.
(45) Wang, Y.; Chen, C.; Chen, W.; Yang, F.; Diao, H. Microstructure and Its High-Temperature Annealing Behaviours of a-Si:O:H Film. *Acta Phys. Sin.* **2001**, *50*, 2418.
(46) Jurgens, T. A.; Rogers, J. J. Reactions of Tetraethoxysilane Vapor on Polycrystalline Titanium Dioxide. *J. Phys. Chem.* **1995**, *99*, 731−743.

DOI: 10.1021/acsami.5b03319
ACS Appl. Mater. Interfaces 2015, 7, 15368−15379

(47) Hitchman, M. L.; Alexandrov, S. E. New Approaches to Titania and Silica Cvd. *Electrochem. Soc. Interface* **2001**, *10*, 40−45.
(48) Lee, J.; Li, H.; Lee, W. Y. Thermal Stability of a Chemically Vapor Deposited Multilayer Coating Containing Amorphous Silica and Rutile Titania on Hi-Nicalon Fiber. *J. Am. Ceram. Soc.* **2003**, *86*, 1797−1799.
(49) Habibovic, P.; Barrere, F.; Blitterswijk, C. A.; Groot, K.; Layrolle, P. Biomimetic Hydroxyapatite Coating on Metal Implants. *J. Am. Ceram. Soc.* **2002**, *85*, 517−522.
(50) Saito, M.; Fujii, K.; Soshi, S.; Tanaka, T. Reductions in Degree of Mineralization and Enzymatic Collagen Cross-Links and Increases in Glycation-Induced Pentosidine in the Femoral Neck Cortex in Cases of Femoral Neck Fracture. *Osteoporosis Int.* **2006**, *17*, 986−995.
(51) Vila, M.; Caceres, D.; Prieto, C. Mechanical Properties of Sputtered Silicon Nitride Thin Films. *J. Appl. Phys.* **2003**, *94*, 7868−7873.
(52) Ehrlich, H.; Brunner, E.; Simon, P.; Bazhenov, V. V.; Botting, J. P.; Tabachnick, K. R.; Springer, A.; Kummer, K.; Vyalikh, D. V.; Molodtsov, S. L. Calcite Reinforced Silica−Silica Joints in the Biocomposite Skeleton of Deep-Sea Glass Sponges. *Adv. Funct. Mater.* **2011**, *21*, 3473−3481.

DOI: 10.1021/acsami.5b03319
ACS Appl. Mater. Interfaces 2015, 7, 15368−15379